Tumor Delivery of Ultrasound Contrast Agents Using Shiga Toxin B Subunit

Olivier Couture, Estelle Dransart, Sabrina Dehay, Fariba Nemati, Didier Decaudin, Ludger Johannes, and Mickael Tanter

Abstract

The present study demonstrates the targeting of ultrasound contrast agents to human xenograft tumors by exploiting the overexpression of the glycolipid Gb3 in neovasculature. To this end, microbubbles were functionalized with a natural Gb3 ligand, the B subunit of the Shiga toxin (STxB). The targeting of Gb3-expressing tumor cells by STxB microbubbles was first shown by flow cytometry and fluorescence microscopy. A significantly higher proportion of STxB microbubbles were associated with Gb3-expressing tumor cells compared to cells in which Gb3 expression was inhibited. Moreover, ultrasonic imaging of culture plates showed a 12 dB contrast enhancement in average backscattered acoustic intensity on the surface of Gb3-expressing cells compared to Gb3-negative cells. Also, a 18 dB contrast enhancement was found in favor of STxB microbubbles compared to unspecific microbubbles. Microbubble signal intensity in subcutaneous tumors in mice was more than twice as high after the injection of STxB-functionalized microbubbles compared to the injection of unspecific microbubbles. These in vitro and in vivo experiments demonstrated that STxB-functionalized microbubbles bind specifically to cells expressing the Gb3 glycolipid. The cell-binding moieties of toxins thus appear as a new group of ligands for angiogenesis imaging with ultrasound.

MICRON-SIZED GAS BUBBLES are used as ultrasound contrast agents.[1] The high scattering cross section and nonlinear acoustic behavior of microbubbles allow their strong differentiation from tissue echoes.[2] Because of their size, the biodistribution of the contrast agents is limited to the blood pool after injection. Thus, their clinical applications are currently limited to blood flow and perfusion measurements in organs such as the heart,[3] liver,[4] renal transplants,[5] and vascular system.[6]

Microbubbles can also be functionalized by antibodies or receptor ligands.[7] The contrast agent thus acquires an affinity for specific cells, based antigen expression in normal or pathologic tissues. Microbubbles are constrained to the blood vessel lumen and therefore target sites that are present on the accessible surface of vascular endothelial cells,[8] immune cells,[9] or blood clots.[10]

Given that tumor neovascularization is involved in the transition to malignancy, new blood vessels are of particular interest for cancer imaging[11] and possibly therapy.[12] Microbubbles have been successfully targeted to tumor angiogenesis via vascular endothelial growth factor (VEGF) receptors[13] and $\alpha_v\beta_3$-integrin.[14] These targeted ultrasound contrast agents were used to image implanted brain tumors[14] and breast tumors, among others.[13]

Glycolipids are another class of markers for the vascular endothelium of tumors. Indeed, almost all human and animal tumors are characterized by aberrant glycolipid expression.[15] The glycosphingolipid globotriaosylceramide (Gb3 or CD77) is highly expressed on several solid tumors, such as ovarian,[16] testis,[17] breast,[18] and colon tumors,[19,20] and on lymphomas.[21] Of particular interest here, Gb3 was also detected in high amounts on tumor neovasculature.[22–24]

Shiga toxin and the related verotoxins are natural Gb3 ligands. Shiga toxin is produced by *Shigella dysenteriae* and verotoxins by enterohemorrhagic strains of *Escherichia coli*.[24] Verotoxins are responsible for pathologic manifestations that can lead to hemolytic uremic syndrome, the leading cause of pediatric renal failure in the world. These toxins are composed of two subunits: the catalytic A subunit, which modifies ribosomal ribonucleic acid, leading to an inhibition of protein biosynthesis, and the nontoxic homopentameric B subunit (STxB). STxB binds Gb3 and guides the retrograde trafficking of the toxins

DECKER℞

Molecular Imaging, Vol 0, No 0 (month 2010): pp 000–000

1

Molecular Imaging MI_2010_00030.3d 13/4/10 14:04:24
The Charlesworth Group, Wakefield +44(0)1924 369598 - Rev 7.51n/W (Jan 20 2003)

from the plasma membrane to the endoplasmic reticulum via endosomes and the Golgi apparatus.[25] From the endoplasmic reticulum, the catalytic A subunit is retro-translocated to the cytosol.[26]

One pentamer of STxB binds up to 15 Gb3 molecules and demonstrates a high affinity for cells, with Kd values in the nanomolar range.[27] STxB was also shown to be a very stable protein.[28] Moreover, the low immunogenicity of STxB has been demonstrated in mice, and in humans, it was found that patients infected by Shiga toxin–producing bacteria do not develop an antibody response against the B subunit.[29]

Given the expression of Gb3 by tumor cells and the capacity of STxB to cross tissue barriers and to escape from extra- and intracellular inactivation, exploiting the protein as a tumor delivery tool has been suggested.[29] STxB targets spontaneous and xenograft tumors in mice[30] and primary human tumoral enterocytes.[20,24] Therapeutic compositions on the basis of STxB are currently being developed.[31] STxB also targets tumor vasculature in mice.[31–34]

We here explored the possibility of using STxB to functionalize microbubbles for ultrasound contrast imaging of tumor angiogenesis. The specific interaction between Gb3-expressing cells and STxB microbubbles was demonstrated in vitro using immunofluorescence and ultrasound imaging. The STxB microbubble agent was also used in a tumor xenograft model in mice.

Materials and Methods

Cell Culture and Animal Model

For in vitro experiments, colon adenoarcinoma HT29 cells were grown in Dulbecco's Modified Eagle's Medium (DMEM) supplemented with 10% (vol/vol) fetal bovine serum (FBS), 100 units/mL penicillin, 10 μg/mL streptomicin, 4 mM glutamine, and 5 mM sodium pyruvate. For inhibition of Gb3 synthesis, HT29 cells were cultured for 6 days with DL-PPMP (DL-threo-1-phenyl-2-palmitoyla-mino-3-morpholino-1-propanol) at a final concentration of 5 μM. The day before experiments, HT29 cells were seeded in Opticell plates. In these culture dishes, a sterile chamber is confined by two membranes that are treated for optimal cell adhesion. Importantly, these membranes are transparent to both light and ultrasound.

The HBCx-12 tumor specimen that was used in vivo was obtained with consent from a breast cancer patient by surgical resection of the tumor. The tumor sample was established as xenograft by subcutaneous implantation of a tumor fragment into the scapular area of nude mice and sequentially transplanted. HBCx-12 fragments of 30 to 60 mm^3 were grafted subcutaneously in 3- to 5-week-old Swiss nude mice under anesthesia. Animal care was in accordance with the institutional guidelines of the French Ethical Committee and under the supervision of authorized investigators.

Preparation of STxB-Functionalized Fluorescent Microbubbles

The STxB-Cys variant carrying an additional Cys at its C-terminus was coupled to biotin by incubating a molar excess of a polyethylene glycol–maleimido modified biotin at room temperature with STxB-Cys overnight in phosphate-buffered saline (PBS). After dialysis, the protein was conjugated on primary amines to N-hydroxysuccinimide–Alexa Fluor 488 by incubating a sixfold molar excess of the fluorochrome with STxB-biotin for 2 hours at room temperature. Streptavidinated microbubbles (Bracco Research, Plan-les-Ouates, Switzerland) were prepared following the manufacturer's instructions (stock solution: 1.24×10^9 microbubbles per mL). Alexa Fluor 488–STxB–biotin was added to the stock solution of microbubbles in excess to saturate the biotin binding sites of the streptavidin microbubbles (1 μg streptavidin per 100 μL of stock solution of microbubbles). Control microbubbles were prepared by saturating the microbubbles with nonsubstituted biotin (0.02 μg biotin per 100 μL of microbubbles). Microbubbles were incubated with ligands for 20 minutes and washed three times by centrifugation at 100g before observation by fluorescence microscopy.

Flow Cytometry Analysis of Microbubble Binding to HT29 Cells

Five $\times$ 10^5 HT29 cells were treated or not with DL-PPMP, washed two times in PBS supplemented with 3% FBS, incubated for 30 minutes at 4°C with 10 μL of the stock solution of microbubbles, diluted in 100 μL of PBS–3% FBS, washed three times with PBS–3% FBS, and finally resuspended in 500 μL of the same buffer. Cells were then analyzed by flow cytometry with a FACSCalibur flow cytometer (BD Biosciences, San Jose, CA) in the FL1H channel for Alexa Fluor 488 fluorochrome detection.

Fluorescent and Ultrasound Imaging of STxB Microbubbles on Tumor Cells In Vitro

HT29 cells grown in Opticell plates were incubated for 30 minutes at 4°C in 10 mL DMEM–3% FBS containing 200

µL of STxB microbubble or biotin microbubble stock solutions. The cells were placed on top for optimized binding of floating microbubbles. The cells were then washed three times with DMEM–3% FBS. For all subsequent steps, the Opticell plates were inverted to place the cells at the bottom, thereby decreasing contributions from unspecific binding.

For simultaneous observation of microbubbles and cell membranes, HT29 cells were incubated for 1 minute at 4°C with the membrane dye FM4-64 at a final concentration of 5 µg/mL in PBS. The cells were then immediately observed by epifluorescence microscopy.

When devoted to ultrasound imaging, Opticell plates were controlled by epifluorescence microscopy for microbubble binding to cells, without membrane labeling. The plates were then transferred into a water bath and imaged using a 8 MHz linear array of transducers (128 elements) driven by an ultrasound scanner (Supersonic Imagine, Aix-en-Provence, France), with cells facing the bottom surface (Figure 1). Unattached microbubbles that were left after washing floated under the top membrane. Thanks to the axial (along depth axis) resolution of the imaging system, these microbubbles could be resolved from the bottom membrane. Several B-mode images were recorded. All analysis was performed linearly on a multielement radiofrequency signal using *Matlab* (MathWorks, Natick, MA). Microbubbles were distinguished from the plate by differentiation imaging before and after disruption of the contrast agents. Signal intensity was determined from the average echo power of the bottom surface.
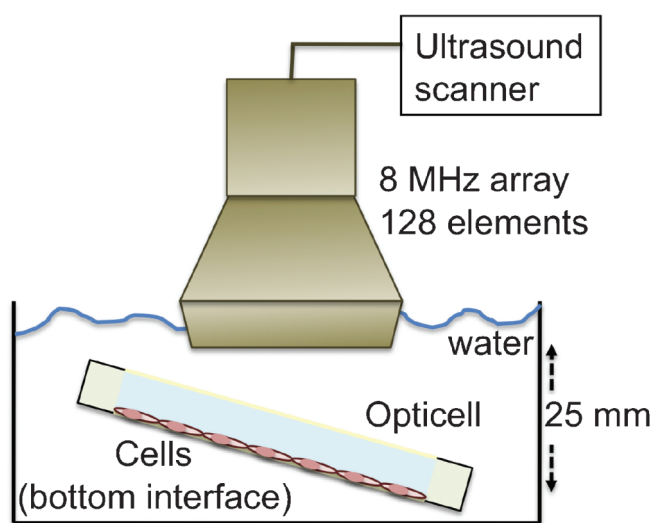
Figure 1. Experimental setup to measure the acoustic reflection of microbubbles attached to cells in an Opticell dish.

Imaging Microbubble Localization onto Tumors In Vivo

Mice bearing HBCx-12 human breast xenograft were anesthetized by intraperitoneal injection of xylazine (10 mg/kg) and ketamine (100 mg/kg). The stock solution of STxB microbubbles was injected in the retro-orbital sinus of the mouse as a bolus of 100 µL ($n = 6$). A control solution of biotin microbubbles was injected similarly in another series of mice ($n = 6$). Mice were placed under an 8 MHz, 256-element ultrasound array (axial resolution ≈ 0.3 mm, pitch ≈ 90 µm) driven by the ultrasound scanner and the imaging plane was aligned with the main axis of the tumor. Using a newly developed harmonic imaging technique,[35] imaging was performed from 5 to 15 minutes postinjection at a rate of four images per minute to prevent destruction of microbubbles. The microbubble attachment dynamics could thereby be monitored (MI = 0.07). Briefly, the well-known amplitude modulation technique for contrast imaging[36] was applied to ultrafast compounded plane wave imaging.[37] Plane wave fronts were generated sequentially by, alternatively, the odd, even, and all elements of the array. These three successive one-cycle emissions were repeated for 17 different angles of plane wave transmissions ranging between −8° and +8°. The final fundamental image was derived from the sum of the echos resulting from the recombination of the 17 different plane wave angles. The harmonic image resulted from a subtraction between the echoes when all elements were firing and the sum of the half-amplitude pulses. Additional image analysis based on angular spectrum bandpass filtering was performed to remove artifacts from specular echoes. The contrast on the harmonic image was established by comparing the echo level to the average into a zone of normal tissue. Linear image intensity was then averaged over a square constrained within the tumor to obtain an absolute value for microbubble accumulation.

Immunohistochemistry of the Expression of Gb3 in Tumor Neovessels

Nude mice bearing HBCx-12 xenograft were injected intravenously with 100 µg of STxB-Cy3 (3.34 mg/kg). Tumors were collected 24 hours postinjection and incubated 3 hours at room temperature in a solution of paraformaldehyde (4% paraformaldehyde in an aqueous solution containing 10 mM PBS, 0.1 mM $CaCl_2$, and 1.0 mM $MgCl_2$). Tumors were stored in sucrose 30%, and 5 µm frozen tumor sections were incubated with monoclonal anti-CD34 (MEC 14.7 clone, Santa Cruz

Biotechnology, Santa Cruz, CA) and secondary donkey antirat IgG coupled to Alexa Fluor 488 (Molecular Probes, Eugene, OR). 4,6-Diamidino-2-phenylindole (DAPI) was used to stain nuclei. Sections were observed under a confocal microscope (TCS SP2, Leica).

Results

In Vitro Targeting of Gb3-Expressing Tumor Cells by STxB-Conjugated Microbubbles

For convenient fluorescent detection of STxB-biotin binding to the surface of microbubbles and binding of targeted microbubbles to cells, STxB was conjugated to the Alexa Fluor 488 fluorophore. Streptavidinated microbubbles were incubated with Alexa Fluor 488–STxB–biotin, leading to the appearance of a specific fluorescence signal on the microbubble membranes (Figure 2), demonstrating that STxB was attached to the surface of the contrast agent. To demonstrate the Gb3-dependent tumor cell binding of STxB microbubbles, we first performed flow cytometry analysis on human colorectal carcinoma HT29 cells that had been incubated or not with an inhibitor of Gb3 synthesis. As shown in Figure 3, the mean was 10-fold higher on Gb3-expressing cells when compared to inhibitor-treated cells, indicating a specific interaction of STxB microbubbles with the cellular glycolipid receptor.

To directly visualize the Gb3-dependent binding of STxB microbubbles to HT29 cells, the cells were seeded in Opticell plates for observation by epifluorescence microscopy after plasma membrane labeling with FM4-64 dye.
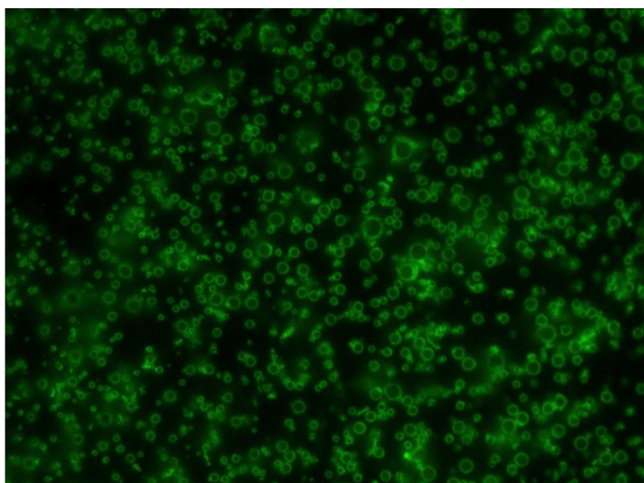
Figure 2. Fluorescence imaging of STxB microbubbles. Alexa Fluor 488–STxB–biotin was incubated with streptavidin-coated microbubbles. Alexa Fluor 488 labeling on the surface of microbubbles could be detected by epifluorescence microscopy (630× magnification).

As shown in Figure 4, STxB-microbubbles were present in greater numbers on the Gb3-expressing cells compared to cells in which Gb3 expression was inhibited. We counted an average of 1.2 microbubbles per Gb3-expressing cell versus 0.2 per Gb3-negative cell ($n = 160$). Moreover, in Gb3-positive HT29 cells, 80% of the microbubbles were in close proximity to the plasma membrane, whereas this number was 25% for inhibitor-treated cells, strongly suggesting that the latter mostly represented situations of nonspecific binding.

Taken together, the flow cytometry and immunofluorescence data demonstrated that STxB mediates Gb3-dependent targeting of microbubbles to cells in vitro.

The Opticell plates were also imaged with ultrasound. Even with disruption imaging, echoes from the Opticell plate membranes were detectable, creating a background signal. Both membranes (2 mm apart) could thereby clearly be distinguished. Cells were placed to face the bottom side, thereby separating floating microbubbles from cell-attached ones. In the first pair of controlled testing (Figure 5, A and B), the average intensity of the echo from the bottom surface was 12 dB higher (fourfold increase) for Gb3-expressing cells compared to inhibitor-treated Gb3-negative cells. More STxB bubbles were thus attached to the cells when the molecular target was present. In the second set of controlled testing (Figure 5, C and D), STxB microbubbles displayed a 18 dB higher (eightfold increase) average intensity than biotin microbubbles when measured over the entire plate. Very clearly, STxB microbubbles were more efficiently targeted than control microbubbles to Gb3-expressing cells.

In Vivo Targeting of Gb3-Expressing Tumors by STxB-Conjugated Microbubbles

In vivo experiments were performed on human breast cancers (HBCX-12) implanted subcutaneously in mice. As STxB microbubbles are expected to target tumor microvasculature, immunohistochemistry was performed on HBCX-12 tumor sections to confirm Gb3 expression by neovessels. As shown in Figure 6, after in vivo injection of Cy3-STxB, specific labeling could be detected at the level of the neovessels, documenting the Gb3 expression in microvasculature in this tumor model.

For in vivo ultrasound imaging on mice, microbubbles were injected in the retro-orbital sinus, a method previously tested with unspecific microbubbles. In preliminary experiments, it was shown that the agents could readily be identified in the liver. Also, these experiments confirmed that the plane wave harmonic imaging techni-
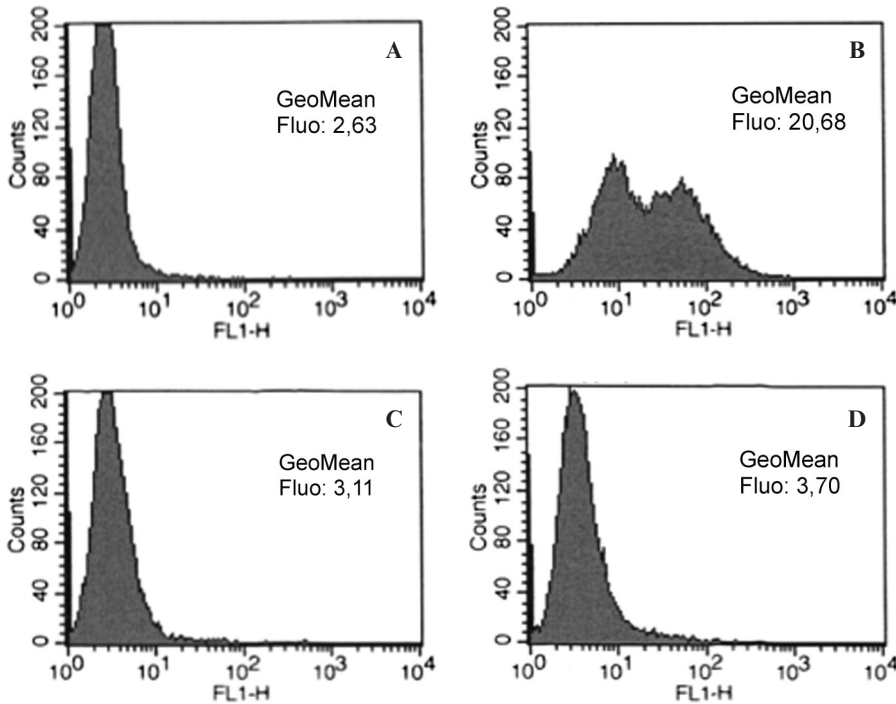
Figure 3. Flow cytometry analysis of STxB microbubble binding to HT29 cells. HT29 cells, nontreated (A, B) or treated with the Gb3 synthesis inhibitor DL-PPMP (C, D), were incubated alone (A, C) or with Alexa Fluor 488–STxB microbubbles (B, D) for 30 minutes at 4°C, washed, and analyzed for microbubbles binding by flow cytometry in the FL1H chanel (Alexa Fluor 488 fluorochrome detection).

que was appropriate to reveal the presence of microbubbles both in vitro and in vivo.

At the time of imaging, xenografted tumors were 5 to 10 mm in diameter. In conventional ultrasound imaging, the tumors were identifiable as hypoechoeic masses compared to the underlying tissue. In Figure 7, microbubble harmonic imaging (*green*) from the dedicated ultrasonic sequence is superimposed to a conventional B-mode image (grayscale). These images were taken 6 minutes after the injection of either STxB microbubbles ($n = 4$, A–D) or biotin microbubbles ($n = 4$, E–H). Contrast enhancement within the core of the tumor was higher for the STxB microbubbles (Figure 8). Indeed, the overall intensity over the whole tumor was more than
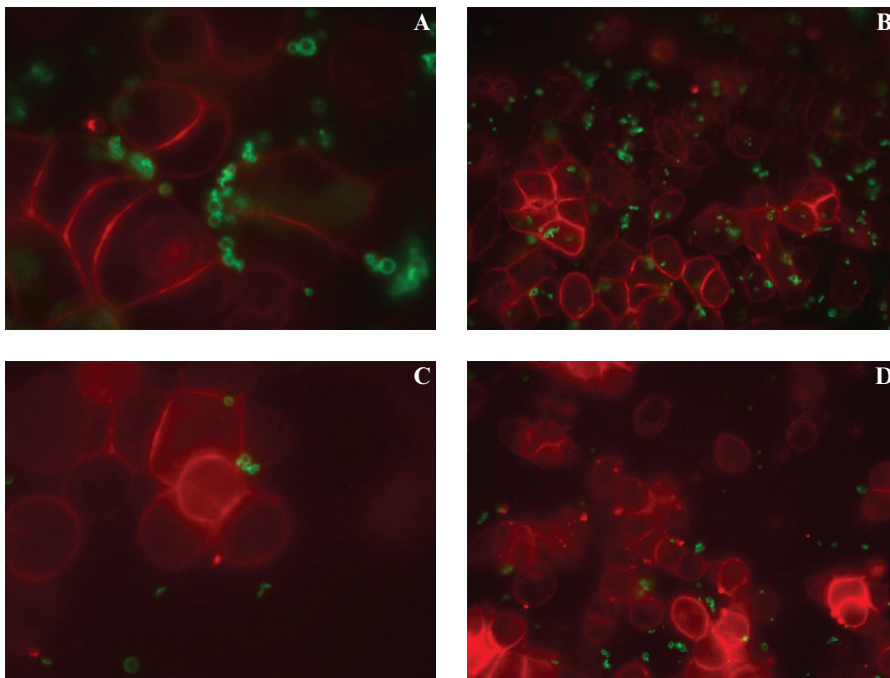
Figure 4. Fluorescence imaging of microbubbles binding to HT29 cells. HT29 cells were treated (C, D) or not (A, B) with the Gb3 synthesis inhibitor DL-PPMP and then incubated with STxB microbubbles for 30 minutes at 4°C. After washing, the cells were incubated for 1 minute at 4°C with FM4-64 for plasma membrane labeling and then observed by fluorescence microscopy (B and D: 40× objective; A and C: 63× objective).
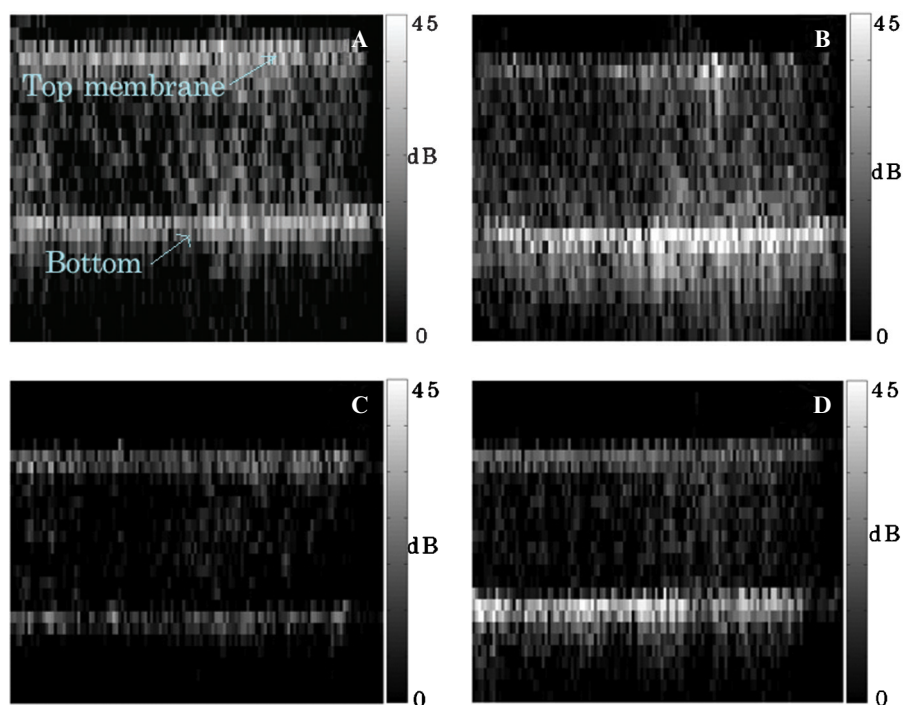
Figure 5. **Ultrasound** scan of an Opticell dish, of which the bottom surface was covered with HT29 cells. STxB microbubbles on Gb3-negative (A) and Gb3-positive (B) cells; biotin microbubbles (C) and STxB microbubbles (D) on Gb3-expressing cells. Not drawn to scale: the images are 4 cm wide, whereas the vertical distance between the membranes is 2 mm. The images of the membrane were also tilted back to the horizontal position.

twice as high for targeted microbubbles, and the two populations formed two distinct groups. Some microbubble contrast was noticeable on the periphery of two tumors injected with unspecific microbubbles.
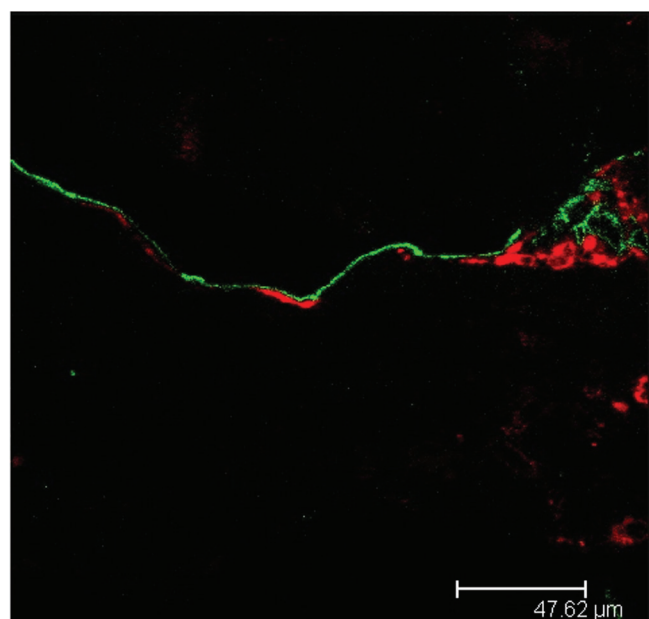
Figure 6. Targeting of HBCX-12 xenografted tumor microvasculature by STxB (*red*). The sections were labeled for the neovessel marker CD34 (*green*).

Discussion

Because of the previously described overexpression of the Shiga toxin receptor Gb3 in tumor neovasculature, we hypothesized that STxB-functionalized microbubbles would preferentially accumulate at sites of tumor growth.

Flow cytometry experiments demonstrated a stable association of fluorescent STxB-microbubbles with Gb3-expressing cells. On the other hand, inhibition of Gb3 synthesis prevented STxB microbubble accumulation on cells, and control microbubbles also failed to bind cells. Fluorescent imaging of cells seeded in Opticell plates confirmed these results and showed significantly higher amounts of STxB microbubbles bound to the surface of Gb3-expressing cells compared to cells in which Gb3 synthesis was inhibited.

Ultrasound experiments performed on the same Opticell plates showed that bubble-specific signal at the bottom of the plate was significantly higher (12 dB or 4 times higher) for Gb3-expressing cells compared to synthesis inhibitor–treated cells and higher for STxB-functionalized microbubbles (18 dB or 8 times higher) compared to biotin microbubbles.

Finally, in vivo experiments performed on mice xenografted with human breast tumors demonstrated a specific tumor accumulation of STxB microbubbles compared to control microbubbles. These results were in good correlation with immunohistochemistry performed on the same tumor after in vivo bioaccumulation of Cy3-
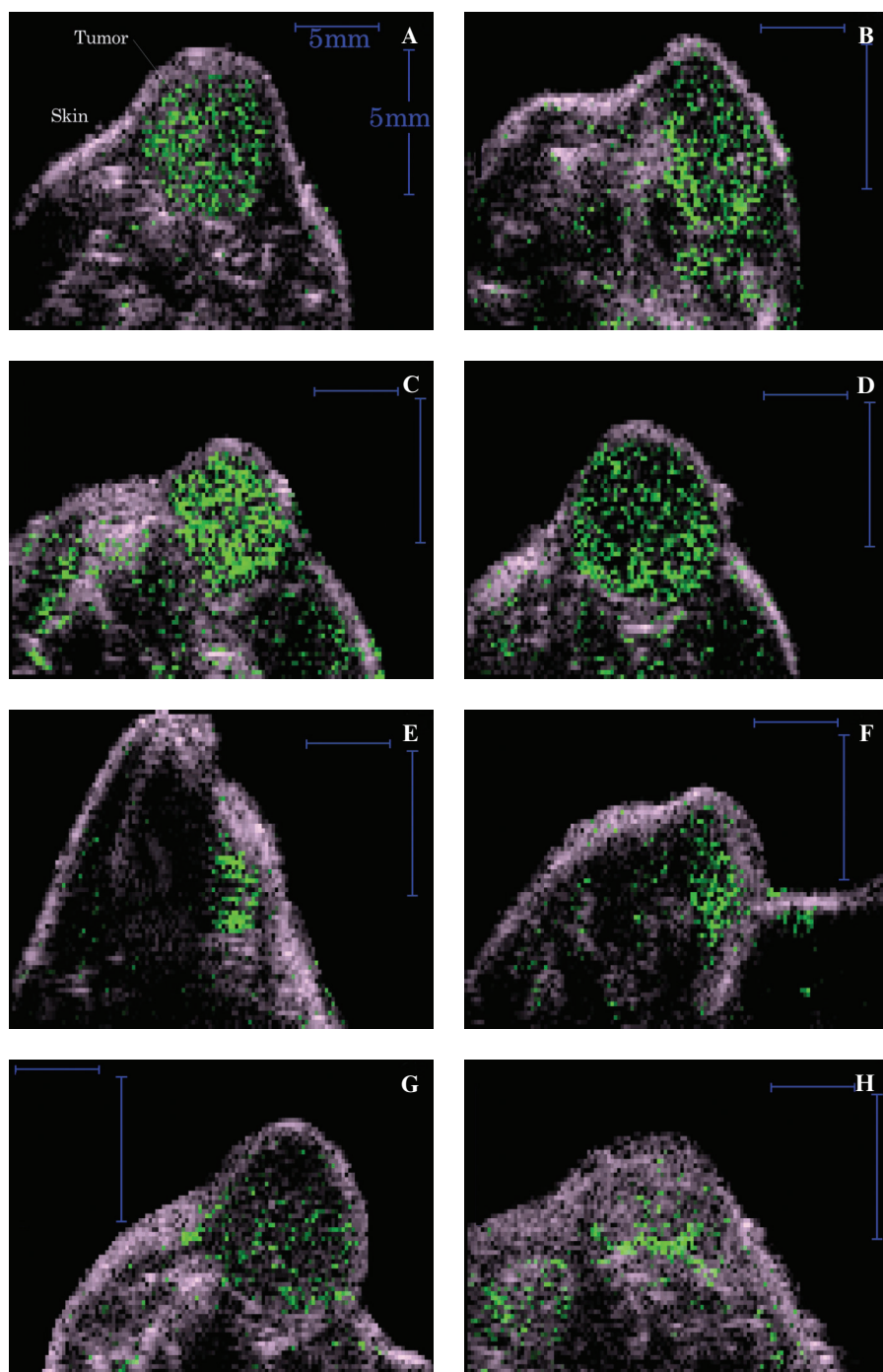
Figure 7. Ultrasound imaging of Gb3-positive HBCX-12 tumors. The four tumors on the *left* (A–D) were images on mice that were injected with STxB microbubbles and those on the *right* (E–H) on mice injected with biotin microbubbles. The *green overlay* is the bubble-specific amplitude modulation signal. The blue scale line is 5 mm across. Images were obtained on eight different mice.

labeled STxB. Indeed, the immunohistochemistry showed a colocalization of STxB with tumor neovessel markers, thus accounting for STxB microbubble targeting to regions of tumor growth.

Altogether, these results demonstrate that STxB microbubbles might be an appropriate tool for investigating tumor angiogenesis. As Shiga toxin has naturally evolved to encounter host defenses, STxB possesses delivery tool properties, such as low immunogenicity and high structural stability in physiologic conditions. Moreover, STxB can be readily produced in and purified from bacteria at gram scales.

In previous studies, we have shown that STxB-functionalized liposomes of smaller size (200 nm) than the microbubbles of the current study (µm scales) are transported inside tumor cells[38] and that they irreversibly
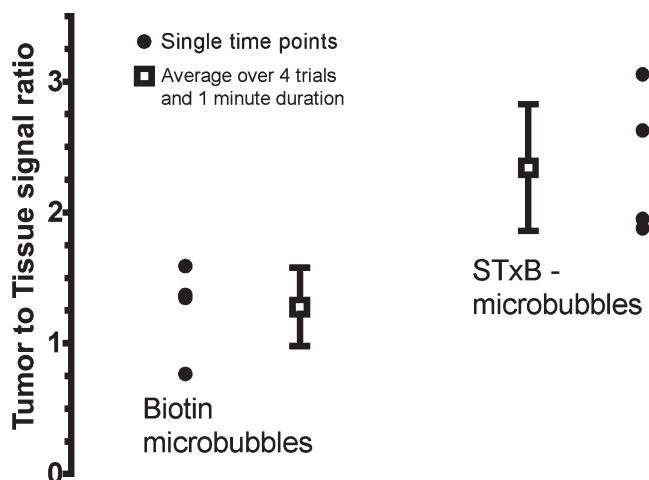
Figure 8. Average intensity of the nonlinear microbubbles echoes over the area of the tumor. The difference between the two sets is statistically significant (unpaired *t*-test, $p < .0001$).

associate with the plasma membrane of these cells in a process that depends in a nonlinear manner on Gb3 expression.[39] Notably, the latter points may be of interest for the development of targeted ultrasound approaches for the following reasons: first, an irreversible adhesion may provide the type of stability in time that is required for combining tumor imaging and therapy (see below). Second, the nonlinear binding dependency on Gb3 expression explains at least in part the fact that STxB targets very few tissues in the organism: although many tissues may express Gb3, only in a few cases (notably in tumors and tumor angiogenesis) are threshold levels of Gb3 expression reached that are required for STxB binding.

Gb3 could thus join other well-known biomarkers of angiogenesis, such as VEGF receptor and $\alpha_v\beta_3$-integrin, and provide complementary information on the disease process, diagnosis, and prognosis. For example, Rychak and colleagues demonstrated selective VEGF receptor–mediated microbubble targeting in mice.[40] Given that VEGF receptor is also used as a target for therapy, the need arises for imaging methods such as STxB-based methodology that are independent from the pathway targeted by the therapy. Thereby, an assessment of changes in tumor angiogenesis in response to treatment could be obtained. Consequently, angiogenesis imaging with STxB microbubbles may improve diagnosis of neoplasia, early detection of metastases, and assessment of novel antiangiogenic therapies. It could also help monitor the effect of STxB-based chemotherapy.[32,34]

Future investigations will consist in generating a covalent bond between STxB and the microbubbles to improve the blood stability of the conjugate. The experiments will also be performed at higher frequencies to improve the resolution of the ultrasound system. Counting tools will be introduced to link the linear microbubble signal intensity with the number of contrast agent accumulated in the tumor. The binding dynamic of the microbubbles in the tumor will be compared to other organs, such as the liver. STxB microbubbles will also be investigated as a tool for molecular focusing therapy previously described by our researchers[41] and for targeted delivery of antiangiogenic compounds.

Conclusion

Microbubbles that are functionalized by STxB bind specifically to cells expressing Gb3, an angiogenesis marker, both in vitro and in vivo. These targeted contrast agents result in hyperechoic signals in ultrasonic contrast images and could be used for molecular imaging of cancer and to guide therapeutic ultrasound procedures.

Acknowledgment

References

1. Qin S, Caskey CF, Ferrara KW. Ultrasound contrast microbubbles in imaging and therapy: physical principles and engineering. Phys Med Biol 2009;54:R27–57.
2. Burns PN, Wilson SR. Microbubble contrast for radiological imaging: 1-principles. Ultrasound Q 2006;22:5–13.
3. Dijkmans PA, Knaapen P, Sieswerda GTJ, et al. Quantification of myocardial perfusion using intravenous myocardial contrast echocardiography in healthy volunteers: comparison with position emission tomography. J Am Soc Echocardiogr 2006;19:285–93.
4. Wilson SR, Burns PN. Microbubble contrast for radiological imaging: 1-applications. Ultrasound Q 2006;22:15–8.
5. Fisher T, Dieckhofer J, Muhler M, et al. The use of contrast-enhanced US in renal transplant. Eur Radiol 2005;15:E109–16.
6. Xiong L, Deng YB, Zhu Y, et al. Correlation of carotid plaque neovascularization detected by using contrast-enhanced US with clinical symptoms. Radiology 2009;251:583–9.
7. Dayton PA, Rychak JJ. Molecular ultrasound imaging using microbubble contrast agents. Front Biosci 2007;12:5124–42.
8. Willmann JK, Cheng Z, Davis C, et al. Targeted microbubbles for imaging tumor angiogenesis: assessment of whole-body distribution with dynamic micro-PET in mice. Radiology 2008;249:212–9.
9. Lindner JR, Coggins MP, Kaul S, et al. Microbubble persistence in the microcirculation during ischemia/reperfusion and inflammation is caused by integrin- and complement-mediated adherence to activated leukocytes. Circulation 2000;101:668–75.

10. Schumann PA, Christiansen JP, Quigley RM, et al. Targeted-microbubble binding selectively to GPIIb IIIa receptors of platelet thrombi. Invest Radiol 2002;37:587–93.

11. Ferrara KW, Merritt CR, Burns PN, et al. Evaluation of tumor angiogenesis with US: imaging, Doppler, and contrast agents. Acad Radiol 2000;7:824–39.

12. Chappell CJ, Price RJ. Targeted therapeutic applications of acoustically active microspheres in the microcirculation. Microcirculation 2006;13:57–70.

13. Lyshchik A, Fleischer AC, Huamani J, et al. Molecular imaging of vascular endothelial growth factor receptor 2 expression using targeted contrast-enhanced high-frequency ultrasonography. J Ultrasound Med 2007;26:1575–86.

14. Ellegala DB, Leong-Poi H, Carpenter JE, et al. Imaging tumor angiogenesis with contrast ultrasound and microbubbles targeted to alpha(v)beta3. Circulation 2003;108:336–41.

15. Hakomori S. Tumor malignancy defined by aberrant glycosylation and sphingo(glyco)lipid metabolism. Cancer Res 1996;56:5309–18.

16. Arab S, Russel E, Chapman WB, et al. Expression of the verotoxin receptor glycolipid, globotriaosylceramide, in ovarian hyperplasias. Oncol Res 1997;9:553–63.

17. Ohyama C, Fukushi Y, Satoh M, et al. Changes in glycolipid expression in human testicular tumor. Int J Cancer 1990;45:1040–4.

18. LaCasse EC, Bray MR, et al. Shiga-like toxin-1 receptor on human breast cancer, lymphoma and myeloma. Blood 1999;94:2901–10.

19. Kovbasnjuk O, Mourtazina R, Baibakov B, et al. The glyco-sphingolipid globotriaosylceramide in the metastatic transformation of colon cancer. Proc Natl Acad Sci U S A 2006;102:19087–92.

20. Falguières T, Maak M, von Weyhern C, et al. Human colorectal tumors and metastases express Gb3 and can be targeted by an intestinal pathogen-based delivery tool. Mol Cancer Ther 2008;7: 2498–508.

21. Kalisiak A, Minniti JG, Oosterwijk E, et al. Neutral glyco-sphingolipid expression in B-cell neoplasms. Int J Cancer 1991; 49:837–45.

22. Hannah MH, Lingwood CA. Verotoxin sensitivity of ECV304 cells in vitro and in vivo in a xenograph tumour model: VT1 as a tumour neovascular marker. Angiogenesis 2003;6:129–41.

23. Lingwood CA. Verotoxin/globotriaosyl ceramide recognition: angiopathy, angiogenesis and antineoplasia. Biosci Rep 1999;19: 345–54.

24. Johannes L, Römer W. Shiga toxins - from cell biology to biomedical applications. Nat Rev Microbiol 2009. [In press].

25. Johannes L, Popoff V. Tracing the retrograde route in protein trafficking. Cell 2008;135:1175–87.

26. Lord JM, Roberts LM, Lencer WI. Entry of protein toxins into mammalian cells by crossing the endoplasmic reticulum mem-

27. St Hilaire PM, Boyd MK, Toone EJ. Interaction of the Shiga-like toxin type-1 b-subunit with its carbohydrate receptor. Biochemistry 1994;33:14452–63.

28. Pina DG, Gomez J, Villar E, et al. Thermodynamic analysis of the structural stability of the Shiga toxin B-subunit. Biochemistry 2003;42:9498–506.

29. Johannes L, Decaudin D. Protein toxins: intracellular trafficking for targeted therapy. Gene Ther 2005;16:1360–8.

30. Janssen KP, Vignjevic D, Boisgard R, et al. In vivo tumor targeting using a novel intestinal pathogen-based delivery approach. Cancer Res 2006;66:7230–6.

31. Viel T, Dransart E, Nemati F, et al. In vivo tumor targeting by the B-subunit of Shiga toxin. Mol Imaging 2008;7:239–47.

32. El Alaoui A, Schmidt F, Amessou M, et al. Shiga toxin-mediated retrograde delivery of a topoisomerase I inhibitor prodrug. Angew Chem Int Ed Engl 2007;46:6469–72.

33. El Alaoui A, Schmidt F, Sarr M, et al. Synthesis and properties of a mitochondrial peripheral benzodiazepine receptor conjugate. Chem Med Chem 2008;3:1687–95.

34. Amessou M, Carez D, Patin P, et al. Retrograde delivery of photosensitizer (TPPp-O-β-GluOH)3 selectively potentiates its photodynamic activity. Bioconjug Chem 2008;19:532–8.

35. Couture O, Bannouf S, Montaldo G, et al. Ultrafast imaging of ultrasound contrast agents. Ultrasound Med Biol 2009;35:1908–16.

36. Brock-Fisher G, Poland M, Rafter P, Mooney M. Experimental observations of the sensitivity and frequency response of the power modulation technique for contrast imaging, Proc Eur Symp Ultrasound Contrast Imaging 2000; 1–77.

37. Montaldo G, Tanter M, Bercoff J, et al. Coherent plane-wave compounding for very high frame rate ultrasonography and transient elastography. IEEE Ultr Ferro Freq Cont 2009;56:489–506.

38. Poirier C, van Effenterre D, Delord B, et al. Specific adsorption of functionalized colloids at the surface of living cells: a quantitative kinetic analysis of the receptor-mediated binding. Biochim Biophys Acta 2008;1778:2450–7.

39. Bouter A, Delord B, Dransart E, et al. Intracellular trafficking of Shiga toxin B-subunit functionalized spherulites. Biol Cell 2008; 100:717–25.

40. Rychak JJ, Graba J, Cheung AM, et al. Microultrasound molecular imaging of vascular endothelial growth factor receptor 2 in a mouse model of tumor angiogenesis. Mol Imaging 2007;6:289–96.

41. Couture O, Aubry JF, Tanter M, Fink M. Time-reversal focusing of therapeutic ultrasound on targeted microbubbles. Appl Phys Lett 2009;94:173901.

Authors Queries

Journal: **Molecular Imaging**
Paper: **MI_2010_00030**
Title: **Tumor Delivery of Ultrasound Contrast Agents Using Shiga Toxin B Subunit**

Dear Author
During the preparation of your manuscript for publication, the questions listed below have arisen. Please attend to these matters and return this form with your proof. Many thanks for your assistance

Query Reference	Query	Remarks
1	AU: Please provide affiliations for all authors, including locations.	
1	AU: Please provide affiliations for all authors, including locations.	
2	AU: Please provide your degrees.	
3	AU: Based on antigen expression? Please clarify.	
4	AU: Please spell out Kd.	
5	AU: Ethical Committee is the full name?	
6	AU: Please spell out MI.	
7	AU: The figure 3B and 3C are reverse, we follow the labels on the images.	
8	AU: You didn't number your figures. The last fig in your file has the same caption as Fig 7. Is it Fig 8?	
9	AU: Bacteria at gram scales? As you meant?	
10	AU: Please confirm that the disclosure is complete and correct.	
11	AU: Please update ref 24 or provide the DOI.	

12	AU: Please provide the vol number for ref 36.	